nature physics

Article

https://doi.org/10.1038/s41567-022-01894-4

Interplay between superconductivity and the strange-metal state in FeSe

Received: 26 April 2022

Accepted: 24 November 2022

Published online: 16 January 2023

Check for updates

Xingyu Jiang[1,2,8], Mingyang Qin[1,2,8], Xinjian Wei[1,8], Li Xu[1,2], Jiezun Ke[3,4], Haipeng Zhu[3,4], Ruozhou Zhang[1,2], Zhanyi Zhao[1,2], Qimei Liang[5], Zhongxu Wei[1,2], Zefeng Lin[1,2], Zhongpei Feng[1,6], Fucong Chen[1,2], Peiyu Xiong[1], Jie Yuan[1,2,6], Beiyi Zhu[1], Yangmu Li[1,2], Chuanying Xi[5], Zhaosheng Wang[5], Ming Yang[3,4], Junfeng Wang[3,4], Tao Xiang[1,2,7], Jiangping Hu[1,2], Kun Jiang[1,2], Qihong Chen[1,2,6] ✉, Kui Jin[1,2,6] ✉ & Zhongxian Zhao[1,2,6]

In contrast to conventional Fermi liquids where resistivity scales quadratically with temperature, unconventional superconductors usually exhibit a normal-state resistivity that varies as a linear function of temperature (T-linear) in the low-temperature limit. This phenomenon, termed as the strange metal, has been extensively studied in cuprates and is thought to be intimately linked to superconductivity. A quantitative description of its relationship with superconductivity is, therefore, of great importance for developing further theoretical understanding; however, so far, comprehensive studies are scarce due to the difficulties in realizing a systematic control of the superconducting state. Here we report the observation of a typical strange-metal behaviour in FeSe, namely, T-linear resistivity, linear-in-field magnetoresistance and universal scaling of magnetoresistance. More importantly, when we tune the superconductivity by ionic-liquid gating, the superconducting transition temperature increases from approximately 10 to 45 K, and the T-linear resistivity coefficient exhibits a quadratic dependence on the critical temperature. This is a ubiquitous feature that describes the relation between these parameters in various systems including overdoped cuprates and Bechgaard salts. This suggests that there may be a universal mechanism underlying the T-linear resistivity and unconventional superconductivity.

Shortly after the discovery of high-temperature superconductivity in cuprates, it was found that their normal states exhibit non-Fermi-liquid transport behaviours, such as a linear-in-temperature (T-linear) resistivity[1–5] and a linear-in-field (H-linear) magnetoresistance (MR)[6–9]. This unusual normal state, called a strange metal, has been observed in many unconventional superconductors including cuprates and Bechgaard salts. In the phase diagram, the strange-metal state often appears in the neighbourhood of the unconventional superconducting dome, indicating that studying the strange-metal state may provide clues towards understanding the microscopic mechanism of unconventional

[1]Beijing National Laboratory for Condensed Matter Physics, Institute of Physics, Chinese Academy of Sciences, Beijing, China. [2]School of Physical Sciences, University of Chinese Academy of Sciences, Beijing, China. [3]Wuhan National High Magnetic Field Center, Huazhong University of Science and Technology, Wuhan, China. [4]School of Physics, Huazhong University of Science and Technology, Wuhan, China. [5]Anhui Province Key Laboratory of Condensed Matter Physics at Extreme Conditions, High Magnetic Field Laboratory of the Chinese Academy of Sciences, Hefei, China. [6]Songshan Lake Materials Laboratory, Dongguan, China. [7]Beijing Academy of Quantum Information Sciences, Beijing, China. [8]These authors contributed equally: Xingyu Jiang, Mingyang Qin, Xinjian Wei. ✉e-mail: qihongchen@iphy.ac.cn; kuijin@iphy.ac.cn;

https://doi.org/10.1038/s41567-022-01894-4

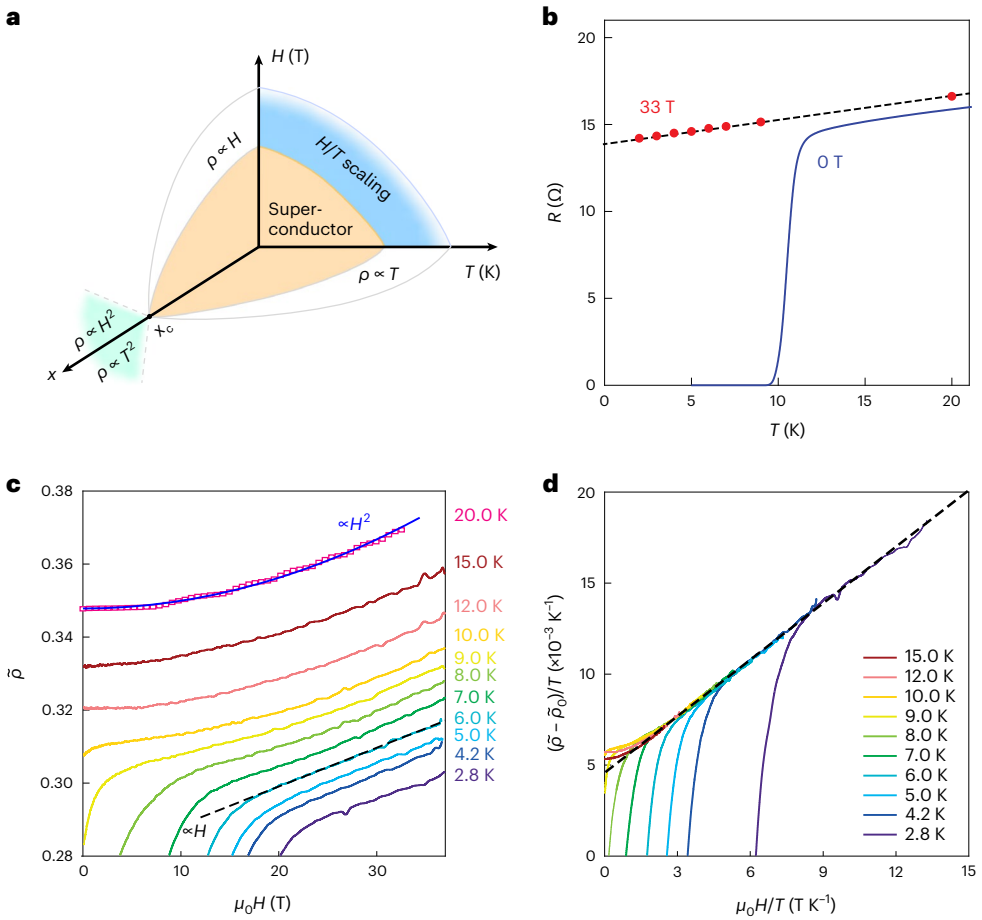

Fig. 1 | Strange metallicity of FeSe. a, Schematic of the general features of the strange-metal state in cuprates as a function of temperature, field and doping. The evolution of linear resistivity as a function of doping is the main subject of this work. **b**, Temperature dependence of the resistance at zero field (solid line) and high field (33 T; red dots). The black dashed line is a guide for *T*-linear resistivity. **c**, Resistivity as a function of magnetic field at different temperatures. The resistivity is normalized by the value at 250 K: $\tilde{\rho} = \rho/\rho\,(250\ \mathrm{K})$. The data from 2.8 to 15.0 K are measured in a pulsed magnet. The data at 20 K (pink squares at the top) are from another sample measured in a steady magnet. As temperature increases, the normal-state MR undergoes a crossover from linear- to quadratic-in-*H* dependence. The black dashed and blue solid lines are fits using linear and H^2 dependences, respectively. **d**, Scaling plot of the MR curves in **c**, where $\tilde{\rho}_0 = \rho(0,0)/\rho\,(250\ \mathrm{K}, 0\ \mathrm{T})$ is the residual resistivity obtained by extrapolating *H*-linear $\tilde{\rho}$ at finite temperatures to $H = 0$ and $T = 0$. The normal-state resistivity is well described by a trendline (black dashed line) proportional to $1 + b(\mu_0 H/T)$, where *b* is a numeric parameter.

superconductivity[10–12]. Nevertheless, despite extensive experimental and theoretical efforts over the past decades, the origin of the strange-metal state and its connection with superconductivity remain major puzzles in condensed-matter physics.

Early on, the strange-metal state was considered to be associated with quantum critical physics[13,14]; yet, in many material families, it was found that *T*-linear resistivity at low temperatures remains robust over a wide doping range[1,2,11]. Such an extended strange-metal regime was further identified by the recent observations of *H*-linear MR at different doping levels in unconventional superconductors such as $BaFe_2(As_{1-x}P_x)_2$ (ref. 6), $La_{2-x}Ce_xCuO_4$ (LCCO) (ref. 8), $Tl_2Ba_2CuO_{6+\delta}$ and (Pb/La)-doped $Bi_2Sr_2CuO_{6+\delta}$ (ref. 11). Intriguingly, a specific H/T scaling of MR was identified in these systems[6,8,11], implying a scale-invariant region where temperature and magnetic field play a similar role in setting an energy scale in transport. Figure 1a summarizes the typical features of strange-metal state and superconductivity in cuprates (in the overdoped regime) as a function of temperature, magnetic field and chemical doping. Importantly, in the strange-metal regime, the *T*-linear resistivity coefficient (namely, A_1 from $\rho = \rho_0 + A_1 T$) is positively correlated with the superconducting transition temperature (T_c) (refs. 2,15), implying a close relationship between *T*-linear resistivity and superconductivity. Since then, there has been concerted effort to quantify the relationship between A_1 and T_c (refs. 1, 7,15), which is of great importance towards a further theoretical understanding. However, establishing a clear quantitative picture has been experimentally challenging due to the lack of systematic data to map across the phase diagrams. Only very recently[16], an explicit expression between A_1 and T_c, namely, $(A_{1\square})^{0.5} = \alpha T_c + \beta$, was uncovered in an electron-doped cuprate LCCO employing a unique composition-spread film fabrication technique. Here, $A_{1\square}$ is the *T*-linear coefficient normalized by the distance between adjacent superconducting layers, and α and β are numeric parameters. A key question is to what extent the power-law dependence between A_1 and T_c can be applied to other systems. It has been found that several other materials, for example, hole-doped cuprates and Bechgaard salts[16], also follow the same trend. However, due to relatively scarce data points, it is hard to conclusively resolve the power-law index for them. Expanding our knowledge of quantitative dependence in different unconventional superconducting systems is highly desired for establishing a unified picture and furthermore promoting our understanding of unconventional superconductivity.

In this work, we investigate this phenomenon in iron-based superconductors—another major class of high-T_c superconductors—in which apart from some fragmented evidence for the strange-metal behaviour in iron pnictides[6,15,17], a comprehensive study of the interplay

between strange-metal state and superconductivity has been lacking. By studying the zero- and high-field electrical transport properties of the iron chalcogenide superconductor FeSe, we obtain clear evidence for strange metallicity in this system, including T-linear resistivity, H-linear MR and linear scaling of MR between T and H. An advantage of FeSe is that its superconductivity can be substantially boosted by electron doping, such as surface K dosing[18], alkali metal/molecule interlayer intercalation[19,20] and ionic-liquid gating[21,22], providing a unique opportunity to explore the evolution of strange metallicity and superconductivity across the phase diagram. Accordingly, we tune the superconductivity of FeSe films employing the ionic-liquid gating technique, which allows a systematic control of the superconducting phase. With the enhancement in T_c from approximately 10 to 45 K, the normal-state resistivity above T_c always exhibits a T-linear characteristic and A_1 shows a quadratic dependence on T_c. A comparison with other systems, including overdoped cuprates (both electron and hole doped) and Bechgaard salts, suggests that a quadratic relation between A_1 and T_c is ubiquitous in unconventional superconductors.

FeSe has the simplest crystal structure in iron-based superconductors, which consists of stacked Fe–Se monolayers. FeSe films ($T_c \approx 10$ K) used in this work, with thicknesses of approximately 200 nm, were grown on LiF or CaF_2 substrates by pulsed laser deposition[23] (Supplementary Section 1). Figure 1b,c shows the in-plane resistivity as a function of temperature and magnetic field, respectively, which exhibit typical features of strange metallicity, namely, T-linear and H-linear resistivity. With superconductivity suppressed by a magnetic field of 33 T, the T-linear resistivity persists to the lowest-measured temperature of 2 K (Fig. 1b). At low temperatures (2.8–6.0 K) the normal-state MR exhibits an H-linear dependence without signs of saturation to the highest-measured field (Fig. 1c). At elevated temperatures (7–15 K), an H^2-dependent MR progressively develops and eventually occupies the whole measured field range (20 K), resembling what is expected in a conventional metal where MR is proportional to H^2. Here, the resistivity is normalized to the value at 250 K (that is, $\tilde{\rho} = \rho(T,H)/\rho(250\,\mathrm{K}, 0\,\mathrm{T})$) to remove the influence of geometric factors, which does not influence any of our analysis.

A scaling analysis is performed for the MR of FeSe similar to previous studies[6,8,11]. Figure 1d shows $(\tilde{\rho} - \tilde{\rho}_0)/T$ versus $\mu_0 H/T$, where $\tilde{\rho}_0$ is the residual resistivity obtained by extrapolating the H-linear $\tilde{\rho}(H, T)$ to zero field and from finite to zero temperature. Evidently, the normal-state resistivity collapses onto a single curve, which is adequately described by the dashed line with the formula $(\tilde{\rho} - \tilde{\rho}_0)/T \propto 1 + b(\mu_0 H/T)$, where b is a numeric parameter. The dashed line agrees well with the experimental data at high H/T values, whereas some deviations occur at very low H/T values. This is because, as mentioned above, there are two components in MR, namely, a linear term (proportional to H) and a quadratic term (proportional to H^2), similar to the observations in $FeSe_{1-x}S_x$ (ref. 9). The scaling only accounts for the H-linear MR at low temperatures and high fields, whereas the H^2 component at high temperatures and low fields cannot be captured by this analysis. This observation is in excellent agreement with the report in LCCO (ref. 8). Consequently, the resistivity can be written as $\rho - \rho_0 \propto Ak_BT + C\mu_B\mu_0 H \equiv \varepsilon(T,H)$, which means that the resistivity is proportional to the linear sum of thermal and magnetic field energies. This suggests that there is a scale-invariant region (Fig. 1a) where the temperature and magnetic field combine to set an energy scale $\varepsilon(T,H)$ in transport. In other words, the lack of an intrinsic energy scale provides a general mechanism for the relaxation rate to scale with external parameters, implying a close relationship between the H-linear and T-linear resistivity behaviours. Overall, the T-linear resistivity, H-linear resistivity and scaling of MR between field and temperature confirm the presence of strange metallicity in the normal state of FeSe, similar to that of cuprates.

To study the interplay between strange metallicity and superconductivity, we tune the superconductivity of FeSe via ionic-liquid gating, which can realize continuous electron doping in a single sample without changing the crystal structure and can be easily integrated with various characterization techniques to probe the evolution of electronic states. The device configuration is shown in Fig. 2a (inset). More details about the device configurations and dimensions can be found in Supplementary Section 2. A gating experiment on a sample includes a set of gating sequences. One sequence includes (1) increasing the gate voltage (V_g) to the desired value, (2) warming up to the gating temperature (T_g), (3) waiting for certain duration time (t_g) and (4) cooling down to measure the superconducting properties.

By adjusting V_g, T_g and t_g, the superconductivity of an FeSe film can be effectively tuned. Figure 2a shows the $\rho(T)$ curves for successive gating sequences of an FeSe film. With gating, the superconducting transition gradually moves to higher temperatures (T_c increases from approximately 10 to 45 K). There are two different scenarios for the gating effect of ionic liquid depending on the gating conditions and materials systems. One is the electrostatic scenario, namely, charge carriers are accumulated near the sample surface due to the electric field effect[24,25], like in a field-effect transistor. In this scenario, only the surface layers are modulated due to the Thomas–Fermi screening effect, where the length scale is about 1 nm. If this is the case, for our 100-nm-thick FeSe films, the inner bulk of the sample remains in the ungated state, which would lead to phase separation. The other scenario involves the electrochemical intercalation of some ionic species throughout the volume of the gated sample[26–28], which results in the bulk modulation of the electronic properties. The actual mechanism would have considerable influence on our analyses of the normal-state resistivity. Therefore, to clarify this issue, we built an in situ two-coil mutual inductance (TCMI) device combined with ionic gating to detect the magnetic response of the sample[29]. Making the TCMI measurement quantitative and operating in situ with ionic-liquid gating have shown great advances in extracting some key information of the superconducting state[30–32]. The variation in mutual inductance, signified by the real part of voltage in the pick-up coil $\mathrm{Re}V_p(T)$, reflects the diamagnetic response of the superconducting state, and therefore, information of the superconducting volume can be extracted. Figure 2b shows the evolution of $\mathrm{Re}V_p(T)$ in successive gating sequences of FeSe (Extended Data Fig. 1 shows the imaginary part of the pick-up voltage). The diamagnetic transition shows a quasi-parallel shift to higher temperatures and each curve exhibits only a single transition, which clearly demonstrates that the gating effect comes from the electrochemical intercalation and whole-sample volume rather than only the surface being modulated. More discussions on the TCMI measurement and the mechanism of ionic-liquid gating can be found in Supplementary Sections 3 and 4.

To examine the strange-metal state with the enhancement in superconductivity, we performed in situ high-field transport measurements with ionic-liquid gating. As shown in Fig. 2c, for the ion-gated state with $T_c \approx 35$ K, under a high field of 50 T, the T-linear resistivity extends to low temperatures, similar to the behaviour in a pristine FeSe film. Data for the high-field measurement of a gated state with $T_c \approx 43$ K can be found in Extended Data Figs. 2 and 3. Here, the magnetic field of 50 T is not enough to completely suppress the superconductivity. It is noteworthy that for another FeSe-based superconductor—(Li,Fe)OHFeSe ($T_c \approx 40.0$ K)[33] that exhibits very similar superconducting properties to ion-gated FeSe, the resistivity shows a T-linear dependence down to 1.4 K when superconductivity is suppressed by a magnetic field of 70 T (Supplementary Section 5), corroborating the T-linear resistivity of FeSe-based superconductors.

For all the $\rho(T)$ curves during gating (Fig. 2a), the normal-state resistivity exhibits a linear dependence on temperature above the superconducting transition. The dashed grey lines (Fig. 2a) are fits for the T-linear resistivity with the function $\rho_n = \rho_0 + A_1 T$. Figure 2d shows the difference (colour map) between experimental data ρ and linear fit ρ_n as a function of electron doping level and temperature. Here, the electron doping level is defined as the electron density induced by ionic-liquid gating, which is roughly estimated via the temporal integral

https://doi.org/10.1038/s41567-022-01894-4

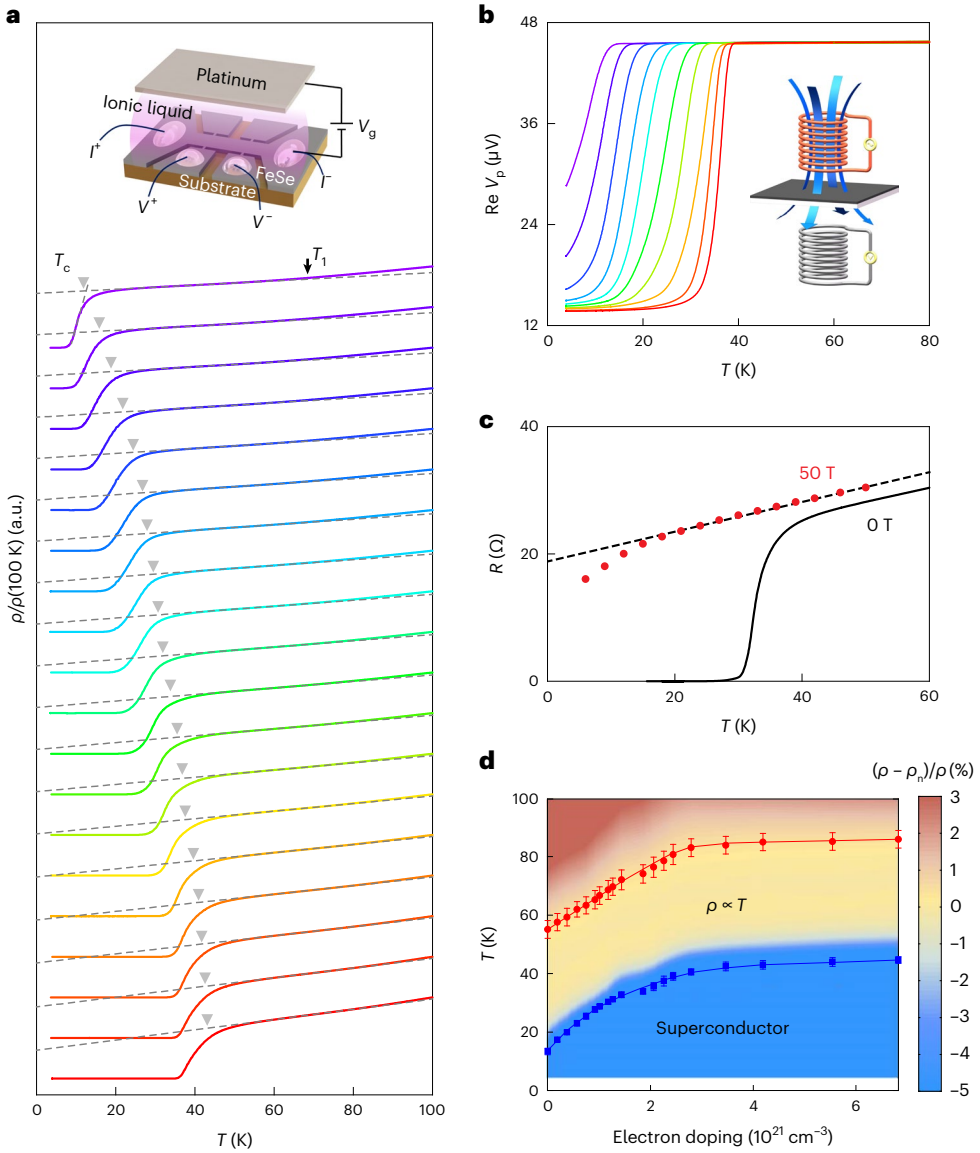

Fig. 2 | Evolution of the superconducting properties of FeSe tuned by ionic-liquid gating. a, Temperature dependence of resistivity for successive gating sequences. The resistivity is normalized by its value at 100 K, and the curves are vertically shifted for comparison. From top to bottom, the gating conditions (V_g, T_g) are (0, 0), (1.50, 280), (1.60, 280), (1.80, 280), (1.90, 280), (2.00, 280), (2.10, 280), (2.20, 280), (2.20, 280), (2.30, 280), (2.40, 280), (2.50, 280), (2.55, 280), (2.65, 280), (2.90, 280), (3.00, 280), (3.00, 282), (3.00, 284) and (3.00, 286); units, (V, K). Here, t_g is 2 h for each state. The grey dashed lines are fits to the normal-state resistivity with the function $\rho_n = \rho_0 + A_1 T$. The inset shows the schematic of the ionic-liquid gating configuration. **b**, Real part of the pick-up signal V_p as a function of temperature in successive gating sequences. From left to right, the gating conditions (V_g, T_g) are (0, 0), (2.70, 270), (2.80, 270), (2.90, 270), (2.95, 270), (3.04, 270), (3.10, 270), (3.10, 275), (3.10, 280) and (3.10, 290); units, (V, K). Here, t_g is 2 h for each state. The inset shows the schematic of the TCMI device. **c**, Temperature dependence of the resistance at zero field (solid line) and high field (50 T; red dots), respectively, for a gated state with $T_c \approx 35$ K. The dashed straight line is a guide for the T-linear resistivity, which extends to low temperatures when superconductivity is suppressed by high magnetic fields. **d**, Colour plot of the difference between experimental data and linear fits of resistivity (that is, $(\rho - \rho_n)/\rho$) versus temperature T and electron doping level. The blue squares and red dots show the evolutions of T_c and T_1 as a function of electron doping level, respectively. T_c is obtained by the intersection of the extrapolation of normal-state resistivity and superconducting transition, as roughly indicated by the inverted triangles in **a**. The error bars for T_c reflect the uncertainty in determining the extrapolation of the superconducting transition. T_1 is determined as the temperature above which $(\rho - \rho_n)/\rho$ exceeds 0.4%. The error bars for T_1 reflect the value where $(\rho - \rho_n)/\rho$ exceeds 0.6%.

of leakage current (Supplementary Section 6). The evolutions of T_c and T_1 are also shown in Fig. 2d. T_c is defined as the onset temperature of the superconducting transition, obtained by the intersection of the extrapolation of normal-state resistivity and superconducting transition (Fig. 2a). T_1 is the upper-bound temperature of T-linear resistivity, determined as the temperature above which the difference between ρ and ρ_n exceeds 0.4%. As T_c gradually increases from approximately 10 to 45 K, T_1 also increases from about 55 to 85 K. Namely, the superconducting regime is enclosed by the T-linear resistivity region. Such an extended electron doping region of T-linear resistivity in FeSe is consistent with the observation of the strange-metal state in a wide doping range of overdoped cuprates, such as hole-doped $La_{2-x}Sr_xCuO_4$ (LSCO) and electron-doped LCCO.

To acquire a quantitative understanding of the relation between the strange-metal state and superconductivity, we extract the T-linear coefficient $A_{1\square}$ from the $\rho(T)$ curves (Fig. 2a) and plot it as a function of T_c (Fig. 3a). Here, $A_{1\square}$ is the slope of the T-linear coefficient normalized by the distance between adjacent Fe–Se layers. As evident from

https://doi.org/10.1038/s41567-022-01894-4

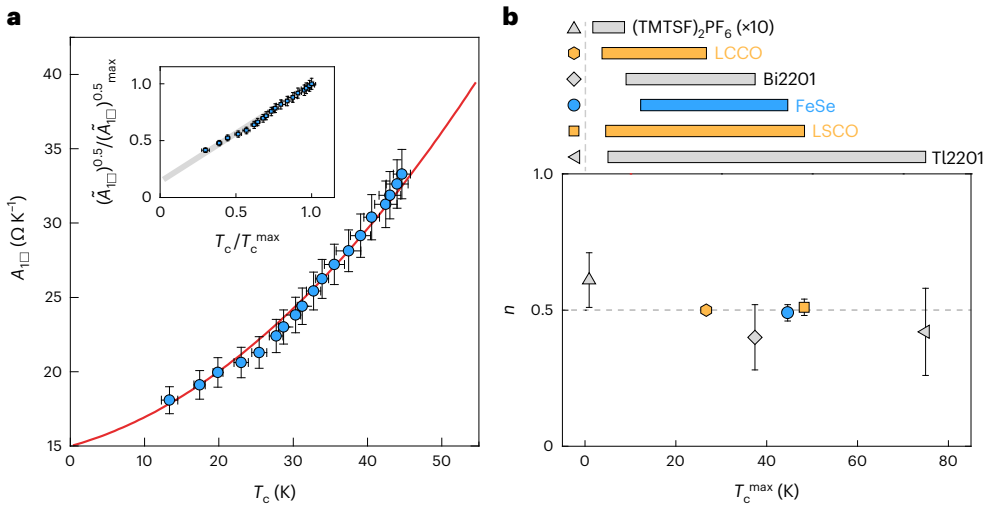

Fig. 3 | Quantitative relation between *T*-linear resistivity and superconductivity. a, *T*-linear coefficient $A_{1\square}$ as a function of T_c extracted from the $\rho(T)$ curves (Fig. 2a). The data show a quadratic dependence on T_c (red line). The inset shows $(\tilde{A}_{1\square})^{0.5}$ as a function of T_c. Here, a constant has been subtracted from $A_{1\square}$, namely, $\tilde{A}_{1\square} \equiv A_{1\square} - A_0$, and the grey line shows the linear fit. The horizontal error bars show the uncertainty in determining T_c, and the vertical error bars originate from the uncertainty in the film thickness and linear fit. **b**, Exponent n extracted for the relationship $(\tilde{A}_{1\square})^n = \alpha T_c + \beta$ as a function of T_c^{max} for different unconventional superconductors (bottom). T_c^{max} corresponds to the maximum value of T_c in each system. Span of T_c for extracting n of the corresponding materials (top). The error bars reflect the fitting uncertainty. The range of $(TMTSF)_2PF_6$ has been multiplied by a factor of 10 for better visualization. The data for LCCO, $Tl_2Ba_2CuO_{6+\delta}$ (Tl2201) and $(TMTSF)_2PF_6$ are extracted from ref. 16 and the references therein; those for LSCO, from ref. 34; and those for (Pb/La)-doped $Bi_2Sr_2CuO_{6+\delta}$ (Bi2201), from ref. 44. The data and fits can be found in Extended Data Fig. 4 and Extended Data Table 1.

the systematic data, the relation between $A_{1\square}$ and T_c is approximately described by a quadratic function (Fig. 3a, red curve). This is reminiscent of the scaling between $A_{1\square}$ and T_c first observed in LCCO, that is, $(A_{1\square})^{0.5} = \alpha T_c + \beta$, which has been shown to be a common relation in several systems[16]. Notably, following the trendline in Fig. 3a, there is an evident non-zero residue for $A_{1\square}$ when extrapolated to $T_c = 0$ K. With a constant (A_0) subtracted, that is, $\tilde{A}_{1\square} \equiv A_{1\square} - A_0$, and fitting with the formula $(\tilde{A}_{1\square})^n = \alpha T_c + \beta$, the extracted value for n is 0.49 ± 0.03, in line with a quadratic dependence between $A_{1\square}$ and T_c. Figure 3b summarizes the exponents extracted for FeSe and several other materials (data from the literature), all of which reside close to 0.5. In particular, the exponent of 0.5 in LCCO has been unambiguously confirmed by a ternary relationship among T_c, $A_{1\square}$ and doping (x), that is, $T_c \propto (A_{1\square})^{0.5} \propto (x - x_c)^{0.5}$ (ref. 16). Here, x_c is the critical doping at the overdoped side where superconductivity disappears. A very similar value is obtained in its hole-doped counterpart, LSCO, in which the data extracted from a comprehensive study[34] yield an exponent of 0.51 ± 0.03.

For LCCO and LSCO, superconductivity is modulated by carrier doping via chemical substitution that takes place in the charge reservoir (La–O) blocks without affecting the Cu–O conducting layers. Likewise, ionic-liquid gating provides a relatively clean method that achieves carrier doping without modifying the Fe–Se conducting layers. As a result, FeSe, LCCO and LSCO show highly consistent exponents close to 0.5 with small uncertainties. It has been discussed[16] that for a hole-doped cuprate $YBa_2Cu_3O_{7-\delta}$, electron irradiation substantially affects T_c but barely changes the slope of *T*-linear resistivity, indicating that disorder can introduce additional effects that result in deviation from the relation obtained in clean compounds. This issue can have a considerable impact on $Tl_2Ba_2CuO_{6+\delta}$ (Tl2201) and (Pb/La)-doped $Bi_2Sr_2CuO_{6+\delta}$ (Bi2201), where T_c is tuned by annealing in oxygen/nitrogen environment that influences the oxygen level of both charge reservoir and conducting layers. It may be one of the reasons that n shows larger uncertainties for these systems. Pressure effectively tunes the superconductivity of $(TMTSF)_2PF_6$, whereas it also modifies lattice parameters that may induce additional electronic states that interact with the strange-metal state and lead to larger uncertainties in determining n. This effect is more evident in high-pressure studies of FeSe, in which magnetic order emerges with the application of small pressures[35], manifested as the anomalies in the $\rho(T)$ curves that obscure the *T*-linear resistivity, and thus, a comprehensive study of the strange-metal state is hindered. Taking these complex facts into account, the overall distribution of n around 0.5 provides adequate evidence that a quadratic dependence is a common feature describing the relation between strange-metal state and superconductivity.

It has been suggested that the *T*-linear resistivity could stem from antiferromagnetic (AF) spin fluctuations[36,37], which has been supported by the experimental findings in Bechgaard salts[38] and electron-doped cuprates[2]. These systems share a similar phase diagram where the superconducting dome emerges at the boundary of the AF regime. Although FeSe does not show any static magnetic order at ambient pressure, the fact that the AF order emerges with the application of a small pressure[35] suggests that the system is in the proximity of a magnetically ordered state and strong AF fluctuations may play an essential role. Indeed, inelastic neutron scattering has revealed that FeSe has a large fluctuating magnetic moment[39,40]. Therefore, the strange-metal behaviours and superconductivity of FeSe could be similarly driven by spin fluctuations associated with short-range AF exchange interactions. This naturally explains the striking similarities between the strange-metal behaviours of overdoped cuprates, Bechgaard salts and ion-gated FeSe in this study. On the other hand, it is widely believed that quantum fluctuations near a quantum critical point could give rise to *T*-linear (*H*-linear) resistivity. However, no signs for magnetic phase transitions have been identified in ionic gating experiments, either in our work or in the literature[21,22,41–43], and therefore, how these phenomena in FeSe are correlated with the quantum critical dynamics remains to be conclusively determined. Besides, there are other scenarios, such as Planckian dissipation[4,10], that have been proposed to explain the strange metallicity. Although the present data do not allow us to distinguish among the various proposed scenarios, the striking similarities found in ion-gated FeSe, overdoped cuprates and Bechgaard salts, are suggestive of a universal mechanism underlying the *T*-linear resistivity and unconventional superconductivity.

A non-zero extrapolation of A_1 to $T_c = 0$ K is seemingly ubiquitous in overdoped cuprates including LCCO (ref. 16), LSCO (ref. 11) and Bi2201 (ref. 44), in which the coefficient of T-linear resistivity retains a finite value when extrapolated to the right-side boundary of the superconducting dome. Taking LCCO as an example, on approaching the right-side boundary of the superconducting dome, T_c decreases more rapidly (that is, $T_c \propto (x_c - x)^{0.5}$), possibly due to strong pairing fluctuations and/or other quantum fluctuations, whereas the T-linear coefficient decreases linearly with doping (that is, $A_1 \propto x$) without showing obvious departure from this trend around x_c. As a result, A_1 retains a finite value close to x_c. However, the magnitude of the extrapolated value for FeSe is seemingly larger than those of cuprates, and after deducting a constant from A_1, FeSe exhibits highly consistent behaviours with LCCO and LSCO. Seemingly, in FeSe, there are T-linear terms in resistivity that are not related to superconductivity and these terms contribute to the large intercept. The origin may lie in the specific electronic structure of FeSe. In contrast to the single-band character of cuprates, for iron-based superconductors, the orbital physics, multiple Fermi surfaces and nematicity have been shown to play important roles in determining their electronic properties[45]. In particular, previous studies have revealed orbital-selective pairing in the superconducting state, and strong orbital-dependent quasiparticle weights in the normal phase[46,47], which are correlated with the enhancement in T_c on electron doping[48]. These effects may lead to the large non-zero A_1 extrapolated to $T_c = 0$ K. Although further investigations are certainly required to understand all these phenomena, the experimental discovery of the common behaviours in T-/H-linear resistivity, MR scaling, and a quadratic dependence between A_1 and T_c in unconventional superconductors has brought us closer to a unified picture.

Online content

Any methods, additional references, Nature Portfolio reporting summaries, source data, extended data, supplementary information, acknowledgements, peer review information; details of author contributions and competing interests; and statements of data and code availability are available at https://doi.org/10.1038/s41567-022-01894-4.

References

1. Cooper, R. A. et al. Anomalous criticality in the electrical resistivity of $La_{2-x}Sr_xCuO_4$. *Science* **323**, 603–607 (2009).
2. Jin, K., Butch, N. P., Kirshenbaum, K., Paglione, J. & Greene, R. L. Link between spin fluctuations and electron pairing in copper oxide superconductors. *Nature* **476**, 73–75 (2011).
3. Bruin, J. A. N., Sakai, H., Perry, R. S. & Mackenzie, A. P. Similarity of scattering rates in metals showing T-linear resistivity. *Science* **339**, 804–807 (2013).
4. Legros, A. et al. Universal T-linear resistivity and Planckian dissipation in overdoped cuprates. *Nat. Phys.* **15**, 142–147 (2019).
5. Licciardello, S. et al. Electrical resistivity across a nematic quantum critical point. *Nature* **567**, 213–217 (2019).
6. Hayes, I. M. et al. Scaling between magnetic field and temperature in the high-temperature superconductor $BaFe(As_{1-x}P_x)_2$. *Nat. Phys.* **12**, 916–919 (2016).
7. Giraldo-Gallo, P. et al. Scale-invariant magnetoresistance in a cuprate superconductor. *Science* **361**, 479–481 (2018).
8. Sarkar, T., Mandal, P. R., Poniatowski, N. R., Chan, M. K. & Greene, R. L. Correlation between scale-invariant normal-state resistivity and superconductivity in an electron-doped cuprate. *Sci. Adv.* **5**, eaav6753 (2019).
9. Licciardello, S. et al. Coexistence of orbital and quantum critical magnetoresistance in $Fe_{1-x}S_x$. *Phys. Rev. Research* **1**, 023011 (2019).
10. Grissonnanche, G. et al. Linear-in temperature resistivity from an isotropic Planckian scattering rate. *Nature* **595**, 667–672 (2021).
11. Ayres, J. et al. Incoherent transport across the strange-metal regime of overdoped cuprates. *Nature* **595**, 661–666 (2021).
12. Putzke, C. et al. Reduced Hall carrier density in the overdoped strange metal regime of cuprate superconductors. *Nat. Phys.* **17**, 826–831 (2021).
13. Daou, R. et al. Linear temperature dependence of resistivity and change in the Fermi surface at the pseudogap critical point of a high-T_c superconductor. *Nat. Phys.* **5**, 31–34 (2009).
14. Analytis, J. G. et al. Transport near a quantum critical point in $BaFe_2(As_{1-x}P_x)_2$. *Nat. Phys.* **10**, 194–197 (2014).
15. Taillefer, L. Scattering and pairing in cuprate superconductors. *Annu. Rev. Condens. Matter Phys.* **1**, 51–70 (2010).
16. Yuan, J. et al. Scaling of the strange-metal scattering in unconventional superconductors. *Nature* **602**, 431–436 (2022).
17. Kasahara, S. et al. Evolution from non-Fermi- to Fermi-liquid transport via isovalent doping in $BaFe_2(As_{1-x}P_x)_2$ superconductors. *Phys. Rev. B* **81**, 184519 (2010).
18. Miyata, Y., Nakayama, K., Sugawara, K., Sato, T. & Takahashi, T. High-temperature superconductivity in potassium-coated multilayer FeSe thin films. *Nat. Mater.* **14**, 775–779 (2015).
19. Guo, J. et al. Superconductivity in the iron selenide $K_xFe_2Se_2$. *Phys. Rev. B* **82**, 180520 (2010).
20. Burrard-Lucas, M. et al. Enhancement of the superconducting transition temperature of FeSe by intercalation of a molecular spacer layer. *Nat. Mater.* **12**, 15–19 (2013).
21. Lei, B. et al. Evolution of high-temperature superconductivity from a low-T_c phase tuned by carrier concentration in FeSe thin flakes. *Phys. Rev. Lett.* **116**, 077002 (2016).
22. Shiogai, J., Ito, Y., Mitsuhashi, T., Nojima, T. & Tsukazaki, A. Electric-field-induced superconductivity in electrochemically etched ultrathin FeSe films on $SrTiO_3$ and MgO. *Nat. Phys.* **12**, 42–46 (2016).
23. Feng, Z. et al. Tunable critical temperature for superconductivity in FeSe thin films by pulsed laser deposition. *Sci. Rep.* **8**, 4039 (2018).
24. Ye, J. T. et al. Superconducting dome in a gate-tuned band insulator. *Science* **338**, 1193–1196 (2012).
25. Chen, Q. H. et al. Inducing and manipulating heteroelectronic states in a single MoS_2 thin flake. *Phys. Rev. Lett.* **119**, 147002 (2017).
26. Jeong, J. et al. Suppression of metal-insulator transition in VO_2 by electric field–induced oxygen vacancy formation. *Science* **339**, 1402–1405 (2013).
27. Lu, N. et al. Electric-field control of tri-state phase transformation with a selective dual-ion switch. *Nature* **546**, 124–128 (2017).
28. Leng, X. et al. Insulator to metal transition in WO_3 induced by electrolyte gating. *npj Quantum Mater.* **2**, 35 (2017).
29. Qin, M. et al. In situ magnetic measurements of ionic-liquid-gated superconducting films. *J. Supercond. Nov. Magn.* **33**, 159–163 (2020).
30. Kinney, J., Garcia-Barriocanal, J. & Goldman, A. M. Homes scaling in ionic liquid gated La_2CuO_{4+x} thin films. *Phys. Rev. B* **92**, 100505 (2015).
31. He, X., Gozar, A., Sundling, R. & Božović, I. High-precision measurement of magnetic penetration depth in superconducting films. *Rev. Sci. Instrum.* **87**, 113903 (2016).
32. Duan, M.-C. et al. Development of in situ two-coil mutual inductance technique in a multifunctional scanning tunneling microscope. *Rev. Sci. Instrum.* **88**, 073902 (2017).
33. Wang, Z. et al. The upper critical field and its anisotropy in $(Li_{1-x}Fe_x)OHFe_{1-y}Se$. *J. Phys. Condens. Matter* **29**, 025701 (2016).
34. Božović, I., He, X., Wu, J. & Bollinger, A. T. Dependence of the critical temperature in overdoped copper oxides on superfluid density. *Nature* **536**, 309–311 (2016).
35. Sun, J. P. et al. Dome-shaped magnetic order competing with high-temperature superconductivity at high pressures in FeSe. *Nat. Commun.* **7**, 12146 (2016).

36. Moriya, T. & Ueda, K. Spin fluctuations and high temperature superconductivity. *Adv. Phys.* **49**, 555–606 (2000).
37. Rosch, A. Magnetotransport in nearly antiferromagnetic metals. *Phys. Rev. B* **62**, 4945–4962 (2000).
38. Doiron-Leyraud, N. et al. Correlation between linear resistivity and T_c in the Bechgaard salts and the pnictide superconductor $Ba(Fe_{1-x}Co_x)_2As_2$. *Phys. Rev. B* **80**, 214531 (2009).
39. Wang, Q. et al. Magnetic ground state of FeSe. *Nat. Commun.* **7**, 12182 (2016).
40. Chen, T. et al. Anisotropic spin fluctuations in detwinned FeSe. *Nat. Mater.* **18**, 709–716 (2019).
41. Hanzawa, K., Sato, H., Hiramatsu, H., Kamiya, T. & Hosono, H. Electric field-induced superconducting transition of insulating FeSe thin film at 35 K. *Proc. Natl Acad. Sci. USA* **113**, 3986–3990 (2016).
42. Ying, T. P. et al. Discrete superconducting phases in FeSe-derived superconductors. *Phys. Rev. Lett.* **121**, 207003 (2018).
43. Shikama, N. et al. Enhancement of superconducting transition temperature in electrochemically etched FeSe/$LaAlO_3$ films. *Appl. Phys. Express* **13**, 083006 (2020).
44. Berben, M. et al. Compartmentalizing the cuprate strange metal. Preprint at https://arxiv.org/abs/2203.04867 (2022).
45. Fernandes, R. M. et al. Iron pnictides and chalcogenides: a new paradigm for superconductivity. *Nature* **601**, 35–44 (2022).
46. Sprau, P. O. et al. Discovery of orbital-selective Cooper pairing in FeSe. *Science* **357**, 75–80 (2017).
47. Si, Q., Yu, R. & Abrahams, E. High-temperature superconductivity in iron pnictides and chalcogenides. *Nat. Rev. Mater.* **1**, 16017 (2016).
48. Villar Arribi, P. & de' Medici, L. Hund-enhanced electronic compressibility in FeSe and its correlation with T_c. *Phys. Rev. Lett.* **121**, 197001 (2018).

Methods

Film growth and characterization

β-FeSe films were grown on (00l)-oriented LiF or CaF_2 substrates by the pulsed laser deposition technique using a KrF excimer laser (λ = 248 nm). The substrates were maintained at 350 °C during growth. The film thicknesses are approximately 200 nm. More details about the fabrication of FeSe films can be found in a previous report[23]. The X-ray diffraction pattern and atomic force microscopy image are shown in Supplementary Section 1.

Ionic-liquid gating and electrical transport measurement

The ionic-liquid gating experiments were performed either in a commercial physical property measurement system or in a Montana cryostation. Generally, the FeSe film was placed at the bottom of a small quartz glass cup and immersed by the ionic liquid *N*,*N*-diethyl-*N*-(2-methoxyethyl)-*N*-methylammonium bis(trifluoromethylsulfonyl) imide. A platinum slice as the gate electrode was fixed to the sidewall of the quartz glass cup, which was mounted on the sample puck and transferred to the physical property measurement system/Montana cryostation. Electrical contacts were made by indium soldering and protected by GE varnish to avoid corrosion by electrochemical reaction. Schematic of the ionic-liquid gating configuration and dimensions of the device are shown in Supplementary Section 2. The sample resistance was measured with a four-terminal geometry, using a Keithley 6221 source meter to supply current and a Keithley 2182 voltage meter to measure the voltage. An external Keithley 2400 source meter was used to apply a bias voltage between the gate electrode and sample and simultaneously monitor the leakage current.

In situ TCMI measurement

To characterize the superconducting volume with ionic-liquid gating, we carried out in situ TCMI measurement[29]. Schematic of the TCMI device can be found in Supplementary Section 3. Both the drive and pick-up coils are sealed in a sapphire block with epoxy and axially aligned with the centre of the FeSe film. The two coils are of the same size: the number of turns is 300, the inner diameter is 0.5 mm and the length is 1.6 mm. The drive and pick-up coils are 1.0 and 0.5 mm, respectively, away from the surface of the FeSe film. An alternating current, with a frequency of 10 kHz and amplitude of 2 mA, is applied to the drive coil using a Stanford Research SR830 lock-in amplifier. The drive current induces a voltage in the pick-up coil, V_p, which is detected using the same lock-in amplifier with a reference phase of 90°. The ReV_p (real part of the pick-up signal) undergoes a sudden drop when the sample becomes superconducting at low temperatures, corresponding to the diamagnetic response of the superconducting state.

Determination of electron doping level

The leakage current is used for estimating the electron doping level. The amount of charge (q_i) injected in each gating sequence (i) can be obtained by integrating the leakage current (I_g) as a function of time (t) in this process: $q_i = \int I_g dt$. The electron doping level (n_m) for sequence m is defined as the sum of the charge accumulated in earlier gating sequences divided by the electron charge (e) and volume (V) of the gated sample: $n_m = \frac{Q_m}{eV} = \frac{\sum_{i \le m} q_i}{eV}$. More details of this calculation can be found in Supplementary Section 6.

Data availability

Source data are provided with this paper. All other data that support the findings of this study are available from the corresponding authors upon reasonable request.

Acknowledgements

We thank R. Yu, H. Xie, D. Zhang, G. Xu, Z. Zhang, G. Zhang, K. Liu, X. Wu, G. He, L. Liang and B. Leridon for stimulating discussions. This work was supported by the National Key Basic Research Program of China (2022YFA1403900 (J.H., Q.C., K. Jiang), 2022YFA1403000 (Q.C.), 2021YFA0718700 (K. Jin), 2017YFA0302900 (T.X., K. Jin)), the National Natural Science Foundation of China (12225412 (K. Jin), 11834016 (K. Jin, J.Y.), 11888101 (T.X.), U1832214 (M.Y., J.W.), 11874359 (Z.W.), 11927808 (K. Jin, J.Y.), 11961141008 (B.Z.) and 12274439 (Y.L.)), the Beijing Nova Program of Science and Technology (Grant No. 20220484014 (Q.C.)), the Strategic Priority Research Program (B) of the Chinese Academy of Sciences (XDB25000000 (K. Jin), XDB33000000 (Q.C.)), Beijing Natural Science Foundation (Z190008 (K. Jin, J.Y., Q.C.)), CAS Project for Young Scientists in Basic Research (2022YSBR-048 (K. Jin, J.Y., Y.L.)). The Key Area Research and Development Program of Guangdong Province (grant no. 2020B0101340002 (K. Jin)). A portion of this work was performed on the Steady High Magnetic Field Facilities, High Magnetic Field Laboratory, Chinese Academy of Sciences, and supported by the High Magnetic Field Laboratory of Anhui Province. The pulsed field measurements were performed at Wuhan National High Magnetic Field Center, Huazhong University of Science and Technology.

Author contributions

Q.C., K. Jin. and Zhongxian Zhao conceived and supervised the project. Q.C., X.J., M.Q. and X.W. performed the electrical transport and TCMI measurements. M.Q. and R.Z. designed the TCMI measurement device. M.Q., L.X. and Q.C. performed the high-magnetic-field measurements, with help from J.K., H.Z., R.Z., Q.L., Z. Wei, P.X., C.X., Z. Wang, M.Y. and J.W. Zhanyi Zhao, Z.L., Z.F. and F.C. synthesized the FeSe films. X.J. and Q.C. analysed the experimental data, with assistance from J.Y., B.Z. and Y.L. T.X., J.H. and K. Jiang contributed to the theoretical discussions. X.J., Q.C. and K. Jin wrote the manuscript with input from all authors.

Competing interests

The authors declare no competing interests.

Additional information

Extended data is available for this paper at https://doi.org/10.1038/s41567-022-01894-4.

Supplementary information The online version contains supplementary material available at https://doi.org/10.1038/s41567-022-01894-4.

Correspondence and requests for materials should be addressed to Qihong Chen or Kui Jin.

Peer review information *Nature Physics* thanks Ivan Bozovic, Luca de' Medici and the other, anonymous, reviewer(s) for their contribution to the peer review of this work.

https://doi.org/10.1038/s41567-022-01894-4

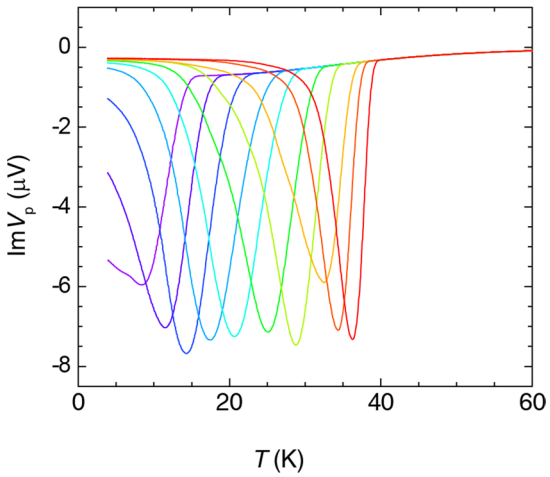

Extended Data Fig. 1 | The imaginary part of the pick-up signal. ImV_p as a function of temperature in successive gating sequences, with one-to-one correspondence (same colour coding) to the data in Fig. 2b of the main text.

https://doi.org/10.1038/s41567-022-01894-4

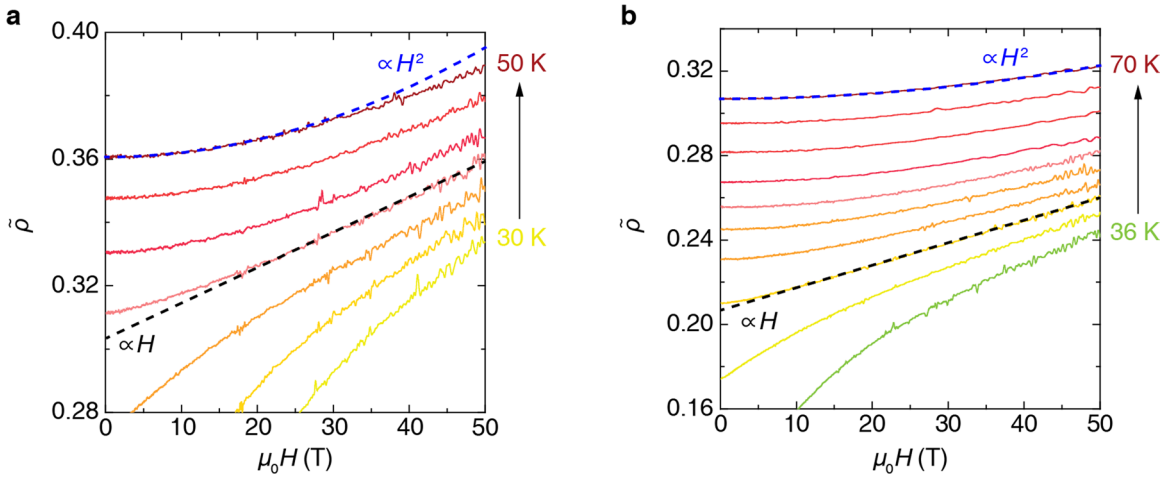

Extended Data Fig. 2 | Linear- to quadratic-in-*H* crossover of MR. Normalized resistivity [$\tilde{\rho} = \rho(T,H)/\rho\,(250\text{K}, 0\text{T})$] as a function of field at different temperatures for a gated FeSe film with **a**, $T_c \approx 35$ K and **b**, $T_c \approx 43$ K. From the bottom to the top curve in each panel, the temperatures are **a**, 30, 33, 36, 39, 42, 46 and 50 K, and **b**, 36, 39, 42, 45, 48, 51, 55, 60, 65 and 70 K. The black dashed and blue dashed lines are fits using linear- and H^2-dependence, respectively.

https://doi.org/10.1038/s41567-022-01894-4

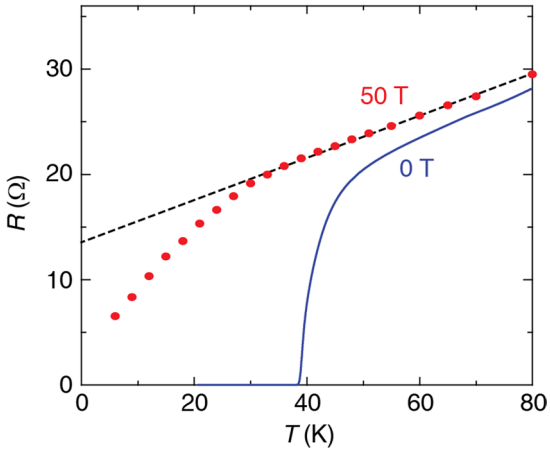

Extended Data Fig. 3 | Normal-state transport of an ion-gated FeSe film. Temperature dependence of resistivity for an ion-gated state with $T_c \approx 43$ K, at 0T (solid line) and 50 T (red dots). The dashed line is a linear guide.

https://doi.org/10.1038/s41567-022-01894-4

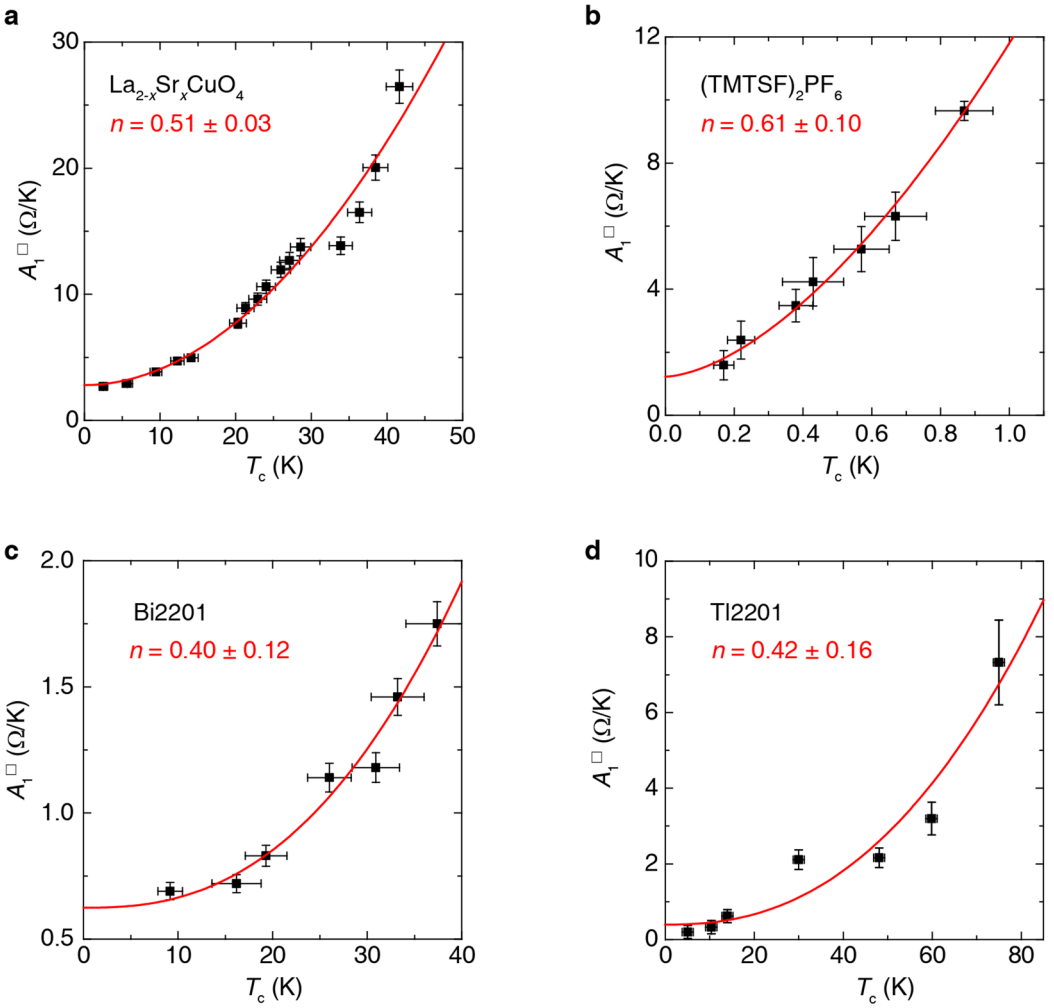

Extended Data Fig. 4 | T_c versus $A_{1\square}$ plots for different unconventional superconductors. Symbols are data extracted from literature and solid curves are fits with the formula $(\tilde{A}_{1\square})^n = \alpha T_c + \beta$, where n is a fitting parameter. Data for $La_{2-x}Sr_xCuO_4$, are extracted from ref. 34; data for $(TMTSF)_2PF_6$ and $Tl_2Ba_2CuO_{6+\delta}$ (Tl2201) are from ref. 16 and references therein; data for (Pb/La)-doped $Bi_2Sr_2CuO_{6+\delta}$ (Bi2201) are extracted from ref. 44. The error bars are reproduced from published data and reflect the uncertainty in determining T_c and the T-linear coefficient.

https://doi.org/10.1038/s41567-022-01894-4

Extended Data Table 1 | Fitting parameters for different unconventional superconductors

Extended Data Table 1 | Fitting parameters for different unconventional superconductors.

	T_c (K)	n	α [$(\Omega/K)^n K^{-1}$]	β [$(\Omega/K)^n$]
Tl2201	74.97	0.42 ± 0.16	0.027 ± 0.001	0.17 ± 0.09
LSCO	48.3	0.51 ± 0.03	0.098 ± 0.004	0.75 ± 0.25
FeSe	44.63	0.49 ± 0.03	0.08 ± 0.002	0.56 ± 0.11
LCCO	26.7	0.50	0.102 ± 0.001	1.22 ± 0.02
Bi2201	37.4	0.4 ± 0.12	0.021 ± 0.003	0.41 ± 0.21
$(TMTSF)_2PF_6$	0.87	0.61 ± 0.1	3.93 ± 0.22	0.61 ± 0.25